

Engineering bands of extended electronic states in a class of topologically disordered and quasiperiodic lattices

Biplab Pal* and Arunava Chakrabarti†

Department of Physics, University of Kalyani, Kalyani, West Bengal-741235, India

We show that a discrete tight-binding model representing either a random or a quasiperiodic array of bonds, can have the entire energy spectrum or a substantial part of it absolutely continuous, populated by extended eigenfunctions only, when atomic sites are coupled to the lattice locally, or non-locally from one side. The event can be fine-tuned by controlling only the host-atom coupling in one case, while in two other cases cited here an additional external magnetic field is necessary. The delocalization of electronic states for the group of systems presented here is sensitive to a subtle correlation between the numerical values of the Hamiltonian parameters – a fact that is not common in the conventional cases of Anderson localization. Our results are analytically exact, and supported by numerical evaluation of the density of states and electronic transmission coefficient.

Keywords: Tight binding model, Delocalization, Single electron states, Ballistic transport

I. INTRODUCTION

Electronic wave functions in a disordered lattice exhibit an exponentially localized envelope in space – a phenomenon, commonly known as the Anderson localization [1–4]. The problem has kept itself alive and kicking over all these years in condensed matter physics, and has given quantum transport properties of disordered systems intriguing twists and turns. The recent development of fabrication and lithographic techniques has taken the phenomenon of Anderson localization beyond the electronic systems, substantiated by remarkable experiments incorporating localization of light [5, 6], ultrasound in three dimensional elastic networks [7], or even plasmonic [8, 9] and polaritonic [10, 11] lattices. Direct observation of the localization of matter waves [12–16] in recent times has made the decades old phenomenon even more exciting.

The key point in Anderson localization is the dimensionality. Within the tight binding approximation, the electronic wave functions are localized for dimensions $d \leq 2$ (the band center in the off diagonal disorder case is an exception). For $d > 2$ with strong disorder, the wave function decays exponentially [2, 3]. Extensive analyses of the localization length [17, 18], density of states [19], and multi-fractality of the single particles states [20, 21] have consolidated the fundamental ideas of disorder induced localization. Intricacies of the single parameter scaling hypothesis – its validity [22], variance [23], or even violation [24, 25] in low dimensional systems provided the finer details of the localization phenomenon that have subsequently been supported by experimental measurements of conductance distribution in quasi-one dimensional gold wires [26].

However, in low dimensions, or more specifically, in one dimensional disordered lattices even a complete delocal-

ization of electronic states can be seen. This path breaking result was initially put forward by Dunlap et al. [27] in connection with a sudden enhancement of conductance of a class of polyanilenes on protonation. Known as the *random dimer model* (RDM) the phenomenon is attributed to certain special kinds of positional correlation in the potential profiles. The investigation of delocalization of eigenstates in correlated disordered models was taken up further over the years and interesting results such as the relation of localization length with the density of states [28] were put forward. The work extended to quasi-one dimensional systems as well for which the Landauer resistance and its relation to the localization length was examined in details [29] for a two-leg ladder model, an extensive extension of which was later done by Sedrakyan et al. [30]. Controlled disorder induced localization and delocalization of eigenfunctions took a considerable volume in contemporary literature, exploring solid non-trivial results involving electron or phonon eigenstates [31–33]. Extended eigenfunctions in all such works mostly appear at special discrete set of energy eigenvalues.

Eventually, the possibility of a controlled engineering of spectral continuum populated by extended single particle states and even a metal-insulator transition in one, or quasi-one dimensional discrete systems have also been discussed in the literature [34–36]. But, on the whole, the general exponentially localized character of the eigenfunctions prevails, and the possibility of having a mixed spectrum of localized and extended states in a disordered system (under some special positional correlations) is now well established.

Can one generate, going beyond the RDM, a full band of only extended eigenfunctions in a disordered system with $d \leq 2$? If yes, what would be the minimal models capable of showing such unusual spectra? This is the question that we address ourselves in the present communication. We put forward examples of a class of essentially one dimensional disordered and quasiperiodic lattices where a *complete delocalization* of electronic states can be engineered, and *absolutely continuous* bands can

*Electronic address: biplabpal@klyuniv.ac.in

†Electronic address: arunava_chakrabarti@yahoo.co.in; Tel.: +91 33 25820184, Fax: +91 33 25828282

be formed in the energy spectrum. This is shown to be possible when an infinite disordered or quasiperiodic array of two kinds of ‘bonds’ is side coupled to a single or a cluster of quantum dots (QD) from one side at a special set of vertices. Minimal requirements are discussed in details. In some of the examples cited here, the attachment of the dots form local loops which can be pierced by a constant magnetic field, breaking the time reversal symmetry of electron-hopping only locally, along the edges of such closed loops. The engineering of bands of extended states is shown to be the result of a definite numerical correlation in the values of the electron hopping amplitude along the chain (backbone) and the coupling of the linear backbone with the side coupled dots, the strength of the magnetic field or both.

It should be mentioned that an early report of a RDM-kind of correlation leading to extended eigenfunctions in a Fibonacci superlattice was put forward by Kumar and Ananthakrishna [37]. The insight into the phenomenon was immediately provided by Xie and Das Sarma [38]. However, the fact that, certain specific *numerical relationship* among a subset of parameters of the Hamiltonian is capable of producing, absolutely continuous *bands* of extended eigenfunctions is uncommon, and to the best of our knowledge, has not been addressed until very recently [39].

We consider two bonds A and B arranged along a line forming an infinite linear chain. The sequence of the bonds may be random or quasiperiodic [40], offering either a pure point spectrum or a singular continuous one. The bonds connect identical atomic sites, an infinite subset of which is coupled to similar atoms (mimicing single level quantum dots (QD)) from one side giving the system a quasi one dimensional flavor. The disorder (or, quasiperiodic order) thus has a topological character. In addition to the basic interest of going beyond the RDM, two other facts motivate us in undertaking such a work.

First, the Fano-Anderson effect [41, 42] caused by the insertion of a bound state into a continuum is an exciting field, and has been investigated recently in nanoscale systems [43]. In this context, our study provides examples where one can observe at least one effect of inserting multiple bound states, in fact, an infinity of them in a *singular continuum*, or a pure point spectrum.

Second, the present advanced stage of growth techniques has motivated in depth studies of quasiperiodic nanoparticle arrays in the context of ferromagnetic dipolar modes [44] or plasmon modes [45]. Also, the use of a scanning tunnel microscope (STM) tip to fabricate structures atom by atom, viz., Xe on Ni substrates [46], or nanometer size gold particles on metals [47], or, putting individual atoms of Si substrate [48] has stimulated a lot of work in this field [49, 50]. Our results can motivate future experiments in this direction.

In section II we describe the lattice models. In Section III, within subsections IIIA and IIIB the local, non-local and the mixed cases introduced in section II are discussed, with explicit remarks on the density of states

profiles in each case. Subsection IIIC specially deals with the special case of a Fibonacci quasiperiodic chain, using a real space renormalization group (RSRG) scheme. Section IV describes the two terminal transmission coefficient, while section V provides a critical discussion on the evolution of the parameter space under the RSRG scheme and its relation with the extendedness of the wave function. In section VI we briefly point out a triplet of other geometries which are less restrictive compared to the ones discussed here, and in section VII we draw our conclusion.

II. THE MODEL

We refer the reader to Fig. 1 where the basic structural units are displayed. The backbone in each case is an infinite array of a single (red) bond B and a double bond A . We shall restrict ourselves to a geometry where the single ‘ B ’ bonds do not come pairwise. Thus we have a kind of ‘anti-RDM’ here. This is not always needed though, as will be discussed in the concluding section.

Three cases are separately discussed. The simplest one is that of a local connection (LC), where a single QD (marked as D in Fig. 1(a) is tunnel-coupled to a site α flanked by two A -bonds. The second case discusses a non-local connection (NLC), where a QD (D) is tunnel-coupled to both the sites residing at the extremities (β and γ in Fig. 1(b)) of a B -bond. The final geometry describes a mixed connection (MC), where two inter-coupled QDs D_1 and D_2 are connected to the extremities of a B -bond (i.e. to β and γ sites) as shown in Fig. 1(c). In the two latter cases a uniform magnetic field is applied in a direction perpendicular to the plane of every closed loop. The system in each case is described by a tight-binding Hamiltonian.

We show that, for a particular algebraic relationship between the nearest neighbor hopping integrals t_{ij} along the backbone and the backbone-QD coupling λ , the infinite topologically disordered or quasiperiodic chain of scatterers yields absolutely continuous energy bands in the spectrum. In the case of LC (Fig. 1(a)) there will be two continuous subbands. In the NLC and MC cases (Fig. 1(b) and (c)) a single absolutely continuous band spans the entire energy spectrum when, in addition to the algebraic relationship between the hopping integrals t_{ij} and λ , the magnetic flux Φ threading each elementary plaquette assumes a particular value. These two cases (NLC and MC) therefore represent situations where the spectral character can be grossly changed from pure point or singular continuous to absolutely continuous by tuning an external magnetic field. This may be useful from the standpoint of device technology.

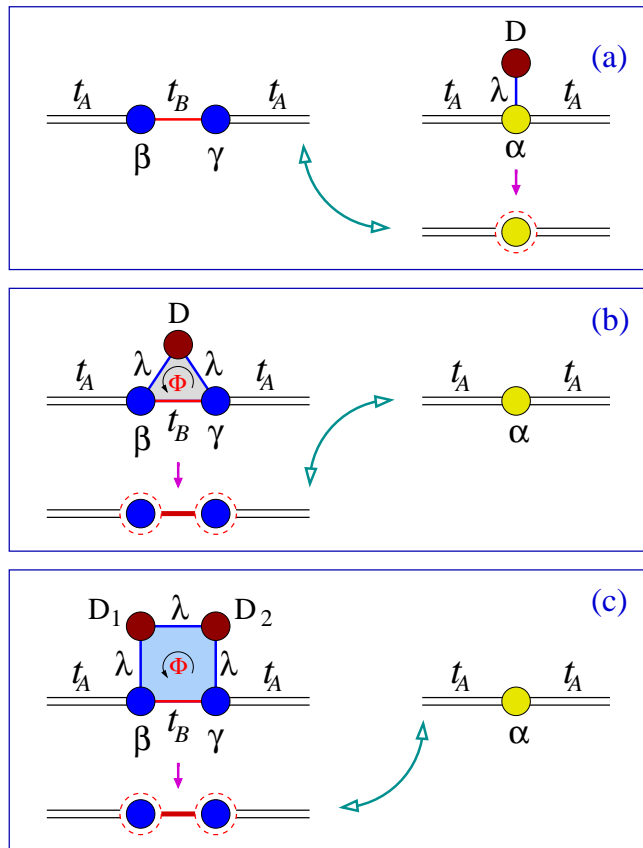


FIG. 1: (Color online) Building blocks of the quasi one-dimensional lattices described in the text. In each case the backbone is a linear array of two kinds of bonds A (double line) and B (red single line), such that a B -bond is always flanked by two A -bonds on either side. The atomic sites on the backbone are marked as α , β and γ as described in the picture. The hopping integrals are appropriately described by t_A and t_B . (a) A QD (D) is locally connected to the α -site. This D - α cluster is “renormalized” into an effective site (yellow circle surrounded by red dotted lines). (b) A QD (D) is non-locally coupled to the β - γ pair. The D - β - γ cluster is then renormalized into the immediate lower geometry, pointed by the arrow. (c) The QDs D_1 and D_2 exhibit a mixed connection to β - γ pair. The block β - D_1 - D_2 - γ is renormalized to the diatomic molecule shown by the arrowhead. In every case, the linear chain (disordered or quasiperiodic) is formed by arranging the cluster linked by the bent cyan double arrowheads in the desired order.

III. THE HAMILTONIAN AND THE GENERAL SCHEME

Spinless, non-interacting electrons on the chain comprising the building blocks depicted in Fig. 1 are described by the Hamiltonian,

$$\mathbf{H} = \epsilon \sum_i c_i^\dagger c_i + \sum_{\langle ij \rangle} t_{ij} [c_i^\dagger c_j + h.c.] \quad (1)$$

where, ϵ is the constant on-site potential, at every site including the QD (marked D). We have colored the

atomic sites differently just to distinguish between their nearest neighbor bond configurations. These are marked as α (yellow circle), β and γ (blue circles) respectively. The nearest-neighbor hopping integral $t_{ij} = t_A$ (double bond) along the backbone on either side of an α -site, while it is t_B (denoted by red line segment) between a β - γ pair. In the LC case (Fig. 1(a)) $t_{ij} = \lambda$ between the QD and the α -site. In the NLC and the MC situations (Fig. 1(b) and (c)) the presence of the magnetic flux breaks the time reversal symmetry along the edges of the loops. This is taken care of by incorporating the appropriate Peierls’ phase factor in the hopping integrals, viz., $t_{ij} \rightarrow t_{ij} \exp(i\theta_{ij})$ where, $\theta_{ij} = 2\pi\Phi a_{ij}/(L\Phi_0)$. L is the perimeter of the plaquette and a_{ij} is the length of the bond connecting the i -th and the j -th sites of the loop. $\Phi_0 = hc/e$ is the flux quantum.

Let us consider symmetric geometries only. This means that, in the NLC case, we assume that the QD is placed symmetrically above the β - γ cluster. In the MC case similarly, the β - D_1 , D_1 - D_2 and the D_2 - γ distances are equal. This just simplifies the mathematical expressions without sacrificing any physics that we are going to establish. Thus, in the NLC (Fig. 1(b)) $t_{\beta\gamma} = t_{\gamma\beta}^* = t_B \exp(i\theta_{1,NL})$, $t_{\gamma D} = t_{D\beta} = t_{\beta D}^* = t_{D\gamma}^* = \lambda \exp(i\theta_{2,NL})$, with $\theta_{1,NL} = 2\pi\Phi a_1/(a_1 + 2a_2)\Phi_0$ and $\theta_{2,NL} = 2\pi\Phi a_2/(a_1 + 2a_2)\Phi_0$, a_1 and a_2 being the bond lengths between the β - γ pair, and the β - D and γ - D pairs respectively. The asterisk denotes the complex conjugate.

Similarly, in the MC case (Fig. 1(c)), $t_{\beta\gamma} = t_B \exp(i\theta_{1,M})$, and $t_{\gamma D_2} = t_{D_2 D_1} = t_{D_1 \beta} = \lambda \exp(i\theta_{2,M})$. In this case however, $\theta_{1,M} = 2\pi\Phi a_1/(a_1 + 3a_2)\Phi_0$ and $\theta_{2,M} = 2\pi\Phi a_2/(a_1 + 3a_2)\Phi_0$ where, a_1 and a_2 are the bond lengths between the β - γ pair, and the β - D_1 , D_1 - D_2 and D_2 - γ pairs respectively. The respective complex conjugates are trivially understood.

Using the difference equation version of the Schrödinger equation, viz.,

$$(E - \epsilon)\psi_i = \sum_j t_{ij}\psi_j \quad (2)$$

we decimate out the vertices (QDs) in each of the three cases to map the local, non-local and mixed clusters on to effective atomic sites with renormalized on-site potentials given by, $\epsilon_\alpha = \epsilon + \lambda^2/(E - \epsilon)$ in the LC (Fig. 1(a)), $\epsilon_\beta = \epsilon_\gamma = \epsilon + \lambda^2/(E - \epsilon)$ in the NLC (Fig. 1(b)), and $\epsilon_\beta = \epsilon_\gamma = \epsilon + \lambda^2(E - \epsilon)/\Delta$ in the MC case (Fig. 1(c)), where, $\Delta = (E - \epsilon)^2 - \lambda^2$. The sites with renormalized on-site potential in each case are encircled with the red dotted lines in Fig. 1. The hopping integrals are still t_A and t_B along the linear backbone for the LC, while they are, $t_{\beta\gamma} = t_{\gamma\beta}^* = t_B \exp(i\theta_{1,NL}) + \lambda^2 \exp(-2i\theta_{2,NL})/(E - \epsilon)$ in the NLC case, and $t_{\beta\gamma} = t_{\gamma\beta}^* = t_B \exp(i\theta_{1,M}) + \lambda^3 \exp(-3i\theta_{2,M})/\Delta$ in the MC case.

One can now build up an infinite chain of α sites (renormalized, in the LC case) and the β - γ doublet (renormalized in the NLC and MC cases) in any desired order. The

amplitude of the wave function at any remote site on such a chain is conveniently obtained by the transfer matrix technique. Using the difference equation the amplitudes of the wave function at the neighboring sites along the effective one dimensional chain can be related using the 2×2 transfer matrices,

$$\begin{pmatrix} \psi_{n+1} \\ \psi_n \end{pmatrix} = \begin{pmatrix} \frac{E - \epsilon_n}{t_{n,n+1}} & -\frac{t_{n,n-1}}{t_{n,n+1}} \\ 1 & 0 \end{pmatrix} \begin{pmatrix} \psi_n \\ \psi_{n-1} \end{pmatrix} \quad (3)$$

The hopping integrals $t_{n,n\pm 1}$ will carry the appropriate phase factors when written for the NLC and MC cases.

It is obvious that there are three kinds of transfer matrices, viz., M_α , M_β , M_γ and which will differ in their matrix elements, depending on the respective on-site potentials and the nearest-neighbor hopping integrals. From the arrangement of the β - γ clusters and the isolated sites in the original chain it can be appreciated that the wave function at a far end of the chain can be determined if one evaluates the product of the unimodular matrices M_α and $M_{\gamma\beta} = M_\gamma \cdot M_\beta$ sequenced in the desired random or quasiperiodic fashion.

The central result of this communication is that, in each of the three cases of LC, NLC and MC, the commutator $[M_\alpha, M_{\gamma\beta}]$ can be made to vanish irrespective of the energy E of the electron whenever the system parameters are inter-related in a certain algebraic fashion. Let us look at the explicit expressions. We list below only one off diagonal element of the commutator for every configuration (LC, NLC or MC), as the diagonal elements of the above commutator vanish identically in each case, and $[M_\alpha, M_{\gamma\beta}]_{21} = [M_\alpha, M_{\gamma\beta}]_{12}$.

- *The Local Coupling:* In this case,

$$[M_\alpha, M_{\gamma\beta}]_{12} = \frac{\lambda^2 - (t_B^2 - t_A^2)}{t_A t_B} \quad (4)$$

- *The Non Local Coupling:* Here,

$$\begin{aligned} [M_\alpha, M_{\gamma\beta}]_{12} = \\ \frac{(E - \epsilon)e^{i2\pi\Phi/\Phi_0}(t_A^2 - t_B^2 - \lambda^2) - 2\lambda^2 t_B \cos(\frac{2\pi\Phi}{\Phi_0})}{t_A e^{i\theta_{1,NL}}[\lambda^2 + (E - \epsilon)t_B e^{i2\pi\Phi/\Phi_0}]} \quad (5) \end{aligned}$$

and,

- *The Mixed Coupling:* In this case,

$$\begin{aligned} [M_\alpha, M_{\gamma\beta}]_{12} = \\ \frac{e^{i2\pi\Phi/\Phi_0}[(E - \epsilon)^2 - \lambda^2](t_A^2 - t_B^2 - \lambda^2) - 2t_B \lambda^3 \cos(\frac{2\pi\Phi}{\Phi_0})}{t_A e^{i\theta_{1,M}} [t_B e^{i2\pi\Phi/\Phi_0} [(E - \epsilon)^2 - \lambda^2] + \lambda^3]} \quad (6) \end{aligned}$$

A look at Eqs. (4)-(6) reveals that it is possible to make the commutator vanish independent of the energy E . Let us discuss case by case.

A. The local coupling

Eq. (4) shows that $[M_\alpha, M_{\gamma\beta}]_{12}$ (and hence the full commutator) vanishes if we set

$$\lambda = \pm \sqrt{t_B^2 - t_A^2} \quad (7)$$

This implies that, with the above value of the tunnel hopping integral, the electronic energy spectrum will no longer be sensitive to the arrangement of the matrices M_α and $M_{\gamma\beta}$, that is, independent of the arrangement of the atomic site α , and the pair β - γ . This happens independent of the energy E of the electron. This result needs to be contrasted clearly with that in the RDM [27] where the local structure of disorder could transform one subset of the transfer matrices into unit matrices, but only at special value of E . In our case, with the commutation condition satisfied one can arrange the constituent elements α and β - γ even in any kind of perfect periodic order. The wave functions as a result, will have to be of a *perfectly extended*, Bloch-like character and the energy bands will exhibit absolutely continuous measure whenever $\lambda = \pm \sqrt{t_B^2 - t_A^2}$. However, this condition is only necessary, and we discuss below the *sufficient* condition for observing extended eigenstates.

Taking advantage of the commutation of the transfer matrices we can shuffle any arrangement of the atoms into two infinite, periodic arrays of the effective renormalized D - α cluster and β - γ clusters (Fig. 2). The local

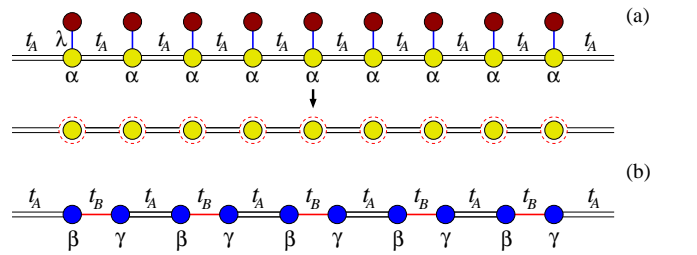


FIG. 2: (Color online) (a) Periodic arrangement of α sites (yellow) coupled to the QD (red) and its renormalized version where the renormalized α sites are encircled by dotted red lines, and (b) periodic array of β - γ pairs. The strength of the hopping t_B (red line) is taken to be greater than t_A (double lines).

density of states (LDOS) at any site of these lattices can be worked out analytically, and for the α and β sites the results are,

$$\begin{aligned} \rho_\alpha &= \frac{1}{\pi} \frac{E - \epsilon}{\sqrt{4t_A^2(E - \epsilon)^2 - [(E - \epsilon)^2 - \lambda^2]^2}} \\ \rho_\beta &= \frac{1}{\pi} \frac{E - \epsilon}{\sqrt{4t_A^2(E - \epsilon)^2 - [(E - \epsilon)^2 - (t_B^2 - t_A^2)]^2}} \quad (8) \end{aligned}$$

In each case, the LDOS exhibits a continuous two-subband structure (typical of a one dimensional binary ordered chain). It is obvious that, with the *resonance*

condition $\lambda = \pm\sqrt{t_B^2 - t_A^2}$ the LDOS in the two cases overlap. That is the bands formed by each individual periodic sublattices merge completely. So, a linear array of the structural units α - D and the β - γ clusters, grown following any chosen pattern (for example, completely disordered, or quasiperiodic geometry) should also exhibit precisely these absolutely continuous subbands. As extended and localized eigenstates can not coexist at the same energy, the electronic states must be of an *extended character*, a fact that is substantiated later by a flow of the hopping integrals under RSRG and a perfect two terminal transmission. This completes the proof that in the LC case, a suitable choice of the hopping integrals can generate absolutely continuous subbands populated only with *extended* single particle states.

B. The non local and the mixed coupling

We now turn our attention to the cases of NLC and MC which essentially refer to an array of triangle shaped and square plaquettes threaded by a magnetic flux and single atomic sites (Fig. 1(b) and (c)). The matrix elements $[\mathbf{M}_\alpha, \mathbf{M}_{\gamma\beta}]_{12}$, as given by Eqs. (5) and (6) become zero in either situation when, $\lambda = \pm\sqrt{t_A^2 - t_B^2}$, and, in

addition to it, $\Phi = \Phi_0/4$ in either case. It means that, even if we fix $\lambda = \pm\sqrt{t_A^2 - t_B^2}$ at the very outset, we still need to tune the magnetic flux Φ through each plaquette to a particular value to have $[\mathbf{M}_\alpha, \mathbf{M}_{\gamma\beta}] = 0$ independent of the energy E of the electron. Just as before, we can now, using the commutivity of \mathbf{M}_α and $\mathbf{M}_{\gamma\beta}$ shuffle the building blocks to generate two infinite periodic chains corresponding to both the NLC and the MC cases, comprising of β - γ pairs, and isolated single sites α ($\epsilon_\alpha = \epsilon$, in both these cases). In terms of the parent lattices, in the NLC situation this means that the single α sites and the β - D - γ triangle can be arranged in any desired pattern, while for the MC case its any arbitrary linear arrangement of the α and the β - D_1 - D_2 - γ cluster.

The α -lattice has the well known density of states, viz., $\rho_\alpha = (1/\pi)[4t_A^2 - (E - \epsilon)^2]^{-1/2}$. To make things look algebraically simple, let us set $\lambda = t_B$, which just means that the side coupled QD is equispaced from the base sites, and that the phase acquired by the electron while hopping along an arm of a triangle as well as of a square is same for all the arms. The resonance condition now boils down to $\lambda = t_B = t_A/\sqrt{2}$ and of course, $\Phi = \Phi_0/4$. The LDOS at the β site corresponding to the NLC case is given by, $\rho_\beta^{NLC} = (1/\pi)(\mathcal{F}_{NLC})^{-1/2}$ where,

$$\mathcal{F}_{NLC} = \frac{4t_A^2 t_B^2 [(E - \epsilon)^2 + 2(E - \epsilon)t_B \cos(2\pi\Phi/\Phi_0) + t_B^2]}{[(E - \epsilon)^2 - t_B^2]^2} \left[E - \frac{\epsilon(E - \epsilon)^2 + 2t_B^3 \cos(2\pi\Phi/\Phi_0) + t_A^2(E - \epsilon) + t_B^2(2E - 3\epsilon)}{(E - \epsilon)^2 - t_B^2} \right]^2 \quad (9)$$

and, the same corresponding to the MC case is given by $\rho_\beta^{MC} = (1/\pi)(\mathcal{F}_{MC})^{-1/2}$ where,

$$\mathcal{F}_{MC} = \xi_1(E, \epsilon, t_A, t_B, \Phi) + \xi_2(E, \epsilon, t_A, t_B, \Phi) \quad (10)$$

ξ_1 and ξ_2 are given by,

$$\begin{aligned} \xi_1(E, \epsilon, t_A, t_B, \theta) &= \frac{4t_A^2 t_B^2 [(E - \epsilon)^4 - 4t_B^2 [(E - \epsilon)^2 - 2t_B^2] \sin^2(\pi\Phi/\Phi_0)]}{(E - \epsilon)^2 [(E - \epsilon)^2 - 2t_B^2]^2} \\ \xi_2(E, \epsilon, t_A, t_B, \theta) &= \left[\frac{(E - \epsilon)(\delta - t_B^2)}{\delta} - \frac{\delta^2(t_A^2 + t_B^2) + t_B^4(t_B^2 + 2\delta \cos(2\pi\Phi/\Phi_0))}{\delta(E - \epsilon)(\delta - t_B^2)} \right] \end{aligned} \quad (11)$$

with $\delta = (E - \epsilon)^2 - t_B^2$.

It is interesting to note that the algebraic expressions in the NLC and MC cases reduce to the simple form $\rho_\alpha = (1/\pi)[4t_A^2 - (E - \epsilon)^2]^{-1/2}$ as soon as we set $\lambda = t_B = t_A/\sqrt{2}$ and $\Phi = \Phi_0/4$. This happens to be the LDOS at the α -site of a pure α -chain. The band extends from $E = \epsilon - 2t_A$ to $E = \epsilon + 2t_A$. Thus, the same resonance condition, viz., $\lambda = t_B = t_A/\sqrt{2}$ and $\Phi = \Phi_0/4$

results in a complete overlap of the energy bands at least in the energy range $[\epsilon - 2t_A, \epsilon + 2t_A]$ in both the cases. We have a single absolutely continuous band of extended eigenfunctions.

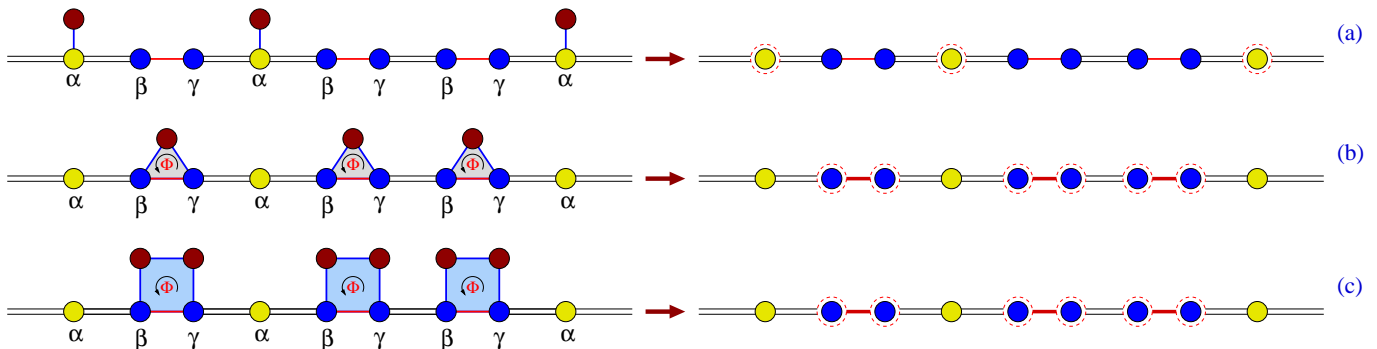


FIG. 3: (Color online) Lattices with the structural units placed in quasiperiodic Fibonacci order along the principal axis (backbone). (a) Local coupling with a QD attached to every α -sites. (b) The non-local coupling and (c) the mixed coupling cases. The linear chains with the renormalized α -sites and the β - γ clusters (or with α -sites and renormalized β - γ doublets), obtained by decimating the QDs (red circle) in every cases are shown for the LC, NLC and MC cases on the right in (a), (b) and (c) respectively.

C. Quasiperiodic Fibonacci order

As a specific example, we explicitly calculate the LDOS at the β -sites in a golden mean Fibonacci quasiperiodic chain. The chain is grown recursively following the usual Fibonacci inflation rule $A \rightarrow AB$ and $B \rightarrow A$ [40]. The corresponding hopping integrals t_A and t_B follow a Fibonacci arrangement. The local, non-local or the mixed attachments of the QDs are shown in Fig. 3. The ‘quasi one-dimensionality’ caused by the side coupled clusters are removed by decimating the attachments and creating an *effective* one dimensional chain in each case, as depicted in the same figure. The decimation results in renormalized values of the on-site potentials at the α -site in the LC case, and at the β , and the γ -sites in the NLC and the MC cases, as already mentioned.

Such a quasiperiodic Fibonacci chain is, by construction, self similar and allows an exact implementation of the RSRG methods. Renormalized versions of the Fibonacci chain are obtained by the well known decimation scheme [51]. For the sake of understanding and to facilitate a subsequent discussion on the flow in parameter space we present the explicit RSRG recursion relations connecting the $(n+1)$ -th and the n -th stages of iteration for the three cases.

◆ The Local Connection:

$$\begin{aligned}
 \epsilon_{\alpha,n+1} &= \epsilon_{\gamma,n} + \frac{t_{A,n}^2 + t_{B,n}^2}{E - \epsilon_{\beta,n}} \\
 \epsilon_{\beta,n+1} &= \epsilon_{\gamma,n} + \frac{t_{B,n}^2}{E - \epsilon_{\beta,n}} \\
 \epsilon_{\gamma,n+1} &= \epsilon_{\alpha,n} + \frac{t_{A,n}^2}{E - \epsilon_{\beta,n}} \\
 t_{A,n+1} &= \frac{t_{A,n}t_{B,n}}{E - \epsilon_{\beta,n}} \\
 t_{B,n+1} &= t_{A,n}
 \end{aligned} \tag{12}$$

with, $\epsilon_{\alpha,0} = \epsilon + \lambda^2/(E - \epsilon)$, $\epsilon_{\beta,0} = \epsilon_{\gamma,0} = \epsilon$, $t_{A,0} = t_A$ and $t_{B,0} = t_B$.

◆ The Non-Local and the Mixed Coupling:

In both these cases, the magnetic flux breaks the time reversal symmetry, but only locally, along the B bonds connecting the β - γ vertices of the linear chain in the right panels of Fig. 3(b) and (c). For this we designate by t_B^f and t_B^b the *forward* and *backward* hopping respectively along the B bond. This naturally takes care of the phase introduced by the field along this segment. The hopping t_A along the A bond, though free from any phase at the bare length scale, picks up phase on renormalization which needs to be taken care of. The recursion relations for both the chains are,

$$\begin{aligned}
 \epsilon_{\alpha,n+1} &= \epsilon_{\gamma,n} + \frac{t_{A,n}^f t_{A,n}^b + t_{B,n}^f t_{B,n}^b}{E - \epsilon_{\beta,n}} \\
 \epsilon_{\beta,n+1} &= \epsilon_{\gamma,n} + \frac{t_{B,n}^f t_{B,n}^b}{E - \epsilon_{\beta,n}} \\
 \epsilon_{\gamma,n+1} &= \epsilon_{\alpha,n} + \frac{t_{A,n}^f t_{A,n}^b}{E - \epsilon_{\beta,n}} \\
 t_{A,n+1}^f &= \frac{t_{A,n}^f t_{B,n}^f}{E - \epsilon_{\beta,n}} \\
 t_{B,n+1}^f &= t_{A,n}^f
 \end{aligned} \tag{13}$$

The complex conjugate hopping integrals are defined appropriately. The initial values are of course different in these two cases, and are given by, $\epsilon_{\alpha,0} = \epsilon$, $\epsilon_{\beta,0} = \epsilon_{\gamma,0} = \epsilon + \lambda^2/(E - \epsilon)$; $t_{A,0}^f = (t_{A,0}^b)^* = t_A$ and $t_{B,0}^f = (t_{B,0}^b)^* = t_B \exp(i\theta) + \lambda^2 \exp(-2i\theta)/(E - \epsilon)$ in the NLC case, while, $\epsilon_{\alpha,0} = \epsilon$, $\epsilon_{\beta,0} = \epsilon_{\gamma,0} = \epsilon + \lambda^2(E - \epsilon)/\Delta$; $t_{A,0}^f = (t_{A,0}^b)^* = t_A$ and $t_{B,0}^f = (t_{B,0}^b)^* = t_B \exp(i\theta) + \lambda^3 \exp(-3i\theta)/\Delta$ and $\Delta = (E - \epsilon)^2 - \lambda^2$ in the MC case. The phase $\theta = 2\pi\Phi/3\Phi_0$ in the NLC case and it is $\theta = 2\pi\Phi/4\Phi_0$ in the MC one. At every stage of renormalization the renor-

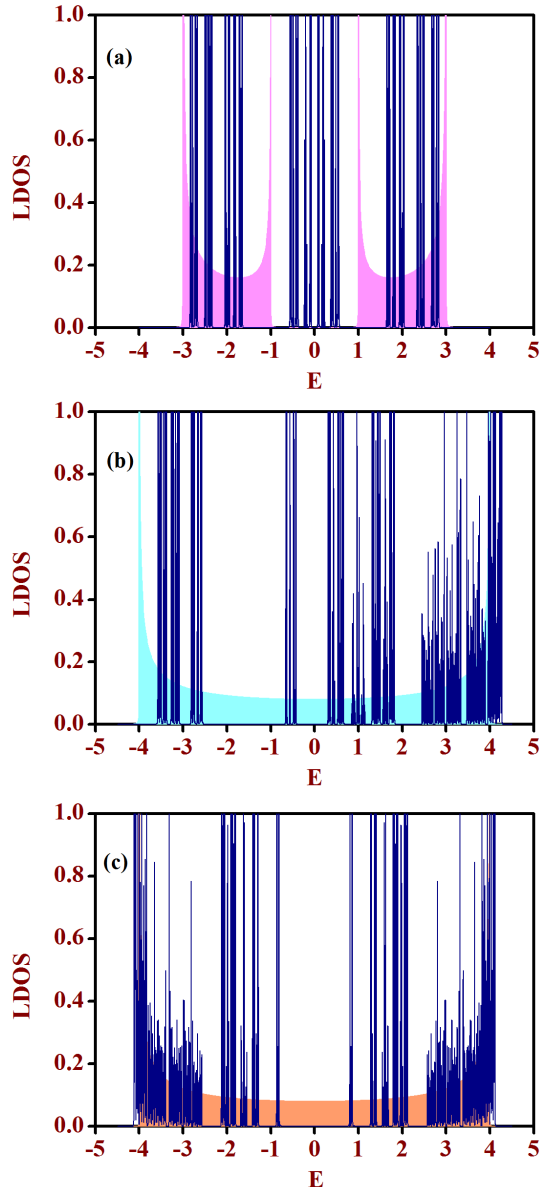


FIG. 4: (Color online) Local density of states (LDOS) at the β site of an infinite Fibonacci array for (a) the locally connected QDs, (b) a single QD non-locally connected to every β - γ pair, and (c) the mixed case of directly and indirectly coupled QDs to the β - γ pair. In each panel, the fragmented display represents the off-resonance case while the absolutely continuous sub-bands or band represent the cases when $[M_{\alpha}, M_{\gamma\beta}] = 0$. We have set $\epsilon = 0$ in all the cases. $t_A = 1$ and $t_B = 2$ in (a) while $t_A = 1$ and $t_B = t_A/\sqrt{2}$ in (b) and (c).

malized *forward* and *backward* hopping integrals are, of course, complex conjugate of each other.

The local Green's function at any j -th site ($j = \alpha, \beta$ or γ) is given by $G_{00} = (E - \epsilon_j^*)^{-1}$ where, ϵ_j^* is the fixed point value of the corresponding on-site potential obtained by repeated application of the set of Eq. (12) and Eq. (13) for the local or the non-local and the mixed cases respectively. The LDOS ρ_j is obtained from the

standard formula $\rho_j = (-1/\pi) \text{Im}[G_{00}(E + i\eta)]$ in the limit $\eta \rightarrow 0$. We present the results in Fig. 4.

In the top panel, the case of LC is shown. The LDOS is obtained at a β -site. The off-resonance case is characterized by the sharp fragmented LDOS profile that brings out the typical multifractal character of the wave functions in a quasiperiodic geometry. As the 'resonance condition' $\lambda = \sqrt{t_B^2 - t_A^2}$ (with $t_B > t_A$) is satisfied, the fragmented spectrum turns into two absolutely continuous subbands.

In the middle and the bottom panels the continuous band in the NLC and MC cases are illustrated by the shaded area. Here we select $t_A > t_B$. The resonance condition in either case is obtained by setting $\lambda = t_B = t_A/\sqrt{2}$ and $\Phi = \Phi_0/4$. Deviating away from this generates the characteristic fragmented spectral form of a Fibonacci chain, as shown by the sharp blue lines (for $\Phi = 0$) in each figure. The interesting difference with the LC case here is the existence of a single continuous band of states which will later be proven as extended, as shown by the shaded colored regions.

It should be appreciated that our purpose has been only to demonstrate the appearance of absolutely continuous part(s) in the energy spectrum. The LDOS coming from any one kind of sites is enough for this purpose. The contribution to the full density of states coming from the side-coupled QD sites generally consists of delta like localized peaks some of which reside outside the continuum [52]. These are of no concern in the present discussion, as the central motivation has always been to prove the generation of a band of extended states only as a result of some algebraic correlation between the numerical values of the parameters of the Hamiltonian. The *extended* character of the eigenstates populating such continuous portions of the energy spectrum will subsequently be discussed in next sections.

IV. TRANSMISSION COEFFICIENT

To substantiate the LDOS profiles we also calculate the two terminal transport in the systems considered. The procedure is standard. The system is clamped between two perfectly periodic, semi-infinite leads on either side (Fig. 5). The sample trapped in between the leads is

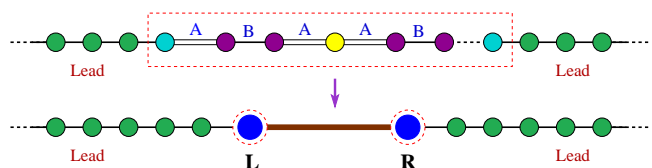


FIG. 5: (Color online) Geometry for calculation of the transmission coefficient. A Fibonacci array of bonds (enclosed in red dashed box) is clamped between two semi-infinite leads (green atoms), which is subsequently renormalized to a *dimer*, shown below by the blue atoms encircled by dotted red lines.

then decimated to a dimer by judiciously using the RSRG recurrence relations. Finally, the transmission coefficient is obtained by the well known formula [53],

$$T = \frac{4 \sin^2 ka}{|\mathcal{A}|^2 + |\mathcal{B}|^2} \quad (14)$$

$$\text{with, } \mathcal{A} = [(P_{12} - P_{21}) + (P_{11} - P_{22}) \cos ka]$$

$$\text{and } \mathcal{B} = [(P_{11} + P_{22}) \sin ka]$$

where, P_{ij} refer to the dimer-matrix elements, written appropriately in terms of the on-site potentials of the final renormalized *left* (L) and *right* (R) atoms ϵ_L and ϵ_R respectively, and the renormalized hopping between them [52]. $\cos(ka) = (E - \epsilon_0)/2t_0$, ϵ_0 and t_0 being the on-site potential and the hopping integral in the leads, and a is the lattice constant in the leads which taken equal to unity throughout the calculation.

In Fig. 6 we plot the transmission coefficient as a function of the energy of the electron in the three cases discussed so far. In each panel, again the resonance and off-resonance cases are plotted together for comparison. In the top panel, for the local coupling, when we set $\lambda = \sqrt{t_B^2 - t_A^2}$, the transmission coefficient attains very high values, achieving the limit unity in most cases for the entire regions of the continuous subbands. There is a clean gap between the two zones of high transmittivity. It is because one has gaps in the energy spectrum in this region, and any *gap states* arising out of the side coupled dots in this part must have a localized character. The perfect transmission under the resonance condition in the LC case brings out a variation over the recent studies of Farchioni et al. [54], where it was rightly shown that, side-coupled dots in general suppress the transmission across a linear tight binding chain.

In the central and the bottom panels, the energy spectrum exhibits a single continuous band spanning the entire energy range. To be consistent with the LDOS figures we have preset $\lambda = t_B = t_A/\sqrt{2}$. The resonance, or a deviation from resonance is now controlled only by controlling the external magnetic field only. When the flux is detuned from its resonance value, the spectrum represents a fragmented character typical of quasiperiodic lattices, while precisely at $\Phi = \Phi_0/4$ the transmission coefficient turns out to be unity for the entire range of the continuum confirming the extended character of the eigenstates.

V. RSRG FLOW PATTERN AND EXTENDEDNESS OF THE EIGENSTATES

In this section we would like to draw the attention of the reader to an interesting flow pattern followed by the on-site potentials and the hopping integrals when the elemental building blocks are arranged in a quasiperiodic Fibonacci chain, as discussed below.

First, it should be noted that, since the transfer matrices M_α and $M_{\gamma\beta}$ corresponding to the structural

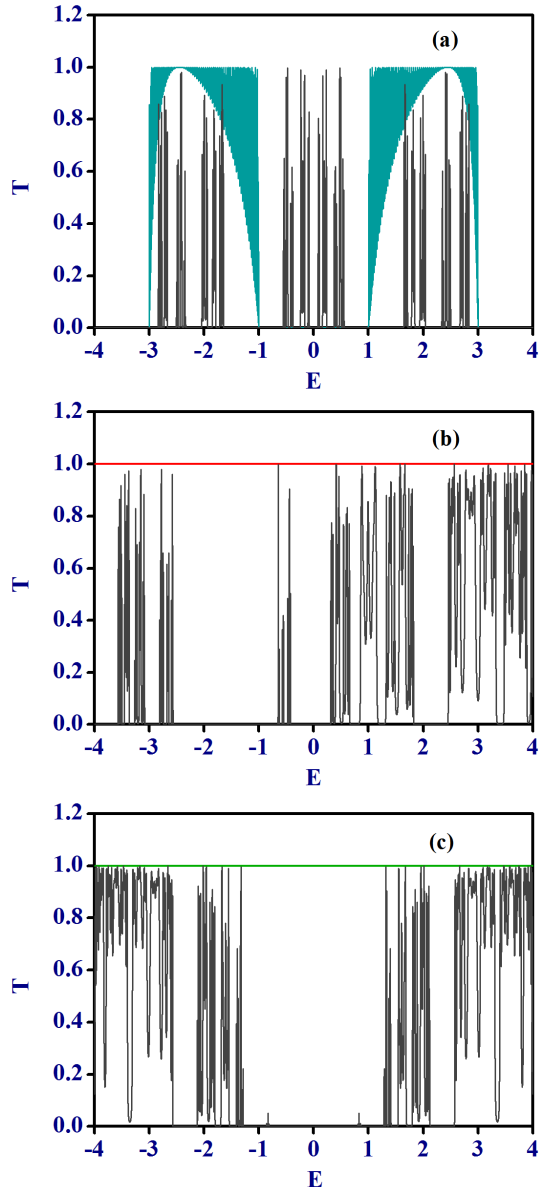


FIG. 6: (Color online) The variation of the transmission coefficient T as a function of the energy E of the electron for both the resonance and the off-resonance conditions. (a) represents the LC case, (b) represents the NLC case and (c) is for the MC case. The numerical values of the potentials and the hopping integrals are the same as in the LDOS figures.

units depicted in Fig. 1(a)-(c) commute independent of energy E under the appropriate *resonance* condition, the energy spectrum in this case should be the same for any uncorrelated disordered or quasiperiodic chains. As far as the quasiperiodic chains are concerned, though we have discussed the results specifically in terms of the golden mean Fibonacci sequence, the idea and subsequent results hold true for any generalized Fibonacci chain grown following the rule $A \rightarrow A^n B$ and $B \rightarrow A$, A and B representing the two bonds and $n \geq 1$.

Second important issue is the confirmation of the ex-

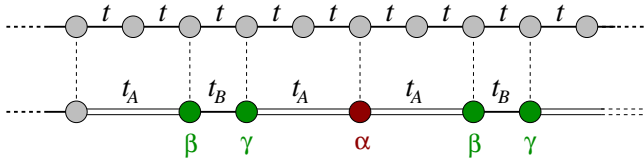


FIG. 7: (Color online) A periodically ordered chain, and a golden mean Fibonacci chain *artificially* generated from it by a selective decimation of sites. The three kinds of sites in the lower chain are α (red), and β and γ (green), and the two nearest neighbor hopping integrals are t_A and t_B respectively.

tended character of the eigenfunctions populating the continuous part of the LDOS spectrum in all the cases. At least, for the deterministic Fibonacci chain (or its generalizations) an interesting answer to this question can be obtained by looking at how the on-site potentials and hopping integrals flow under successive RSRG iterations. Let's try to understand.

In the local coupling case for example, with reference to the Eq. (12), it is found that, as soon as we set $\lambda = \sqrt{t_B^2 - t_A^2}$ the parameter space follows the pattern $\epsilon_\beta(n) = \epsilon_\gamma(n) \neq \epsilon_\alpha(n)$ and $t_A(n) \neq t_B(n)$ at every n -th stage of renormalization, whenever we select an eigenvalue E arbitrarily from within the two continuous subbands in the LDOS spectrum. This observation is substantiated by extensive numerical search throughout the observed continua scanned in arbitrarily small energy intervals. That such a pattern should correspond to extended Bloch-like eigenfunctions can be justified by considering Fig. 7 where a perfectly periodic lattice of identical on-site potential ϵ and a constant nearest neighbor hopping t is artificially converted into a golden mean Fibonacci chain. On this *artificial* Fibonacci chain $\epsilon_{\beta,0} = \epsilon_{\gamma,0} = \epsilon + t^2/(E - \epsilon)$, and different from $\epsilon_{\alpha,0} = \epsilon + 2t^2/(E - \epsilon)$. At the same time, $t_{A,0} = 2t^2/(E - \epsilon) \neq t_{B,0}$, the latter being equal to t . The *flow pattern* that we have been talking about therefore sets in at the very beginning.

The artificial Fibonacci chain in Fig. 7 can now be renormalized using the recursion relations Eq. (12), and the density of states may be obtained from the appropriate Green's function. As the parent lattice now is an ordered one, the typical one dimensional density of states is reproduced with the edges characterized by the van Hove singularity. The spectrum is absolutely continuous, and all the wave functions are Bloch functions. Interestingly, with the initial set of values as given above, the on site potentials and the hopping integrals for the scaled version of the *artificial* Fibonacci lattice (Fig. 7) get locked into the flow pattern $\epsilon_{\beta,n} = \epsilon_{\gamma,n} \neq \epsilon_{\alpha,n}$ and $t_{A,n} \neq t_{B,n}$ at every n -th stage of renormalization, and for all energy eigenvalues within the range $[\epsilon - 2t, \epsilon + 2t]$.

In our actual case of Fibonacci arrangement of the clusters in Fig. 1(a) as soon as such a flow pattern is set in for a special value of λ , it becomes impossible to judge whether the parent lattice was an ordered, perfectly peri-

odic one, or a truly quasiperiodic Fibonacci chain. Thus the extendedness of the wave functions is firmly established whenever such an RSRG flow is observed. Same flow pattern is also observed in the cases of Fig. 1(b) and (c). In these cases, if we set beforehand $\lambda = t_B = t_A/\sqrt{2}$, then the *desired* flow of the parameters can be achieved by tuning the external flux to $\Phi = \Phi_0/4$. This refers to the interesting case of a *flux driven crossover* in the fundamental character of the wave functions in a non-locally coupled case or in the mixed case. In addition, for both the NLC case and the MC case, the LDOS at the β , γ or α sites turn out to be exactly same whenever the resonance condition is satisfied. This is remarkable. The NLC and MC lattices are topologically different. An equality of the LDOS for $\lambda = t_B = t_A/\sqrt{2}$ and $\Phi = \Phi_0/4$ implies that for both these cases the parameters $(\epsilon_\alpha, \epsilon_\beta, \epsilon_\gamma, t_A, t_B)$, initially represented by two different *points* (as their initial values are different) in the five dimensional parameter space, are driven to the same *fixed point* following two different trajectories.

As we have already mentioned, the result is independent of the order of arrangement of the triangles or the square boxes. Thus, for the same resonance condition an indefinite number of geometrically different systems, beginning their 'journey' at different locations in the five dimensional parameter space finally flow, following different trajectories, to the same fixed point, and thus come under the common umbrella. We are tempted to conceptualize a kind of *universality class* from this point of view. It is to be noted however, that the comment is based on the observed LDOS at the sites on the backbone only. The average density of states can be different though.

VI. OTHER GEOMETRIES

Before we end, it should be mentioned that, the central idea presented in the present work is not restricted to only the geometries discussed here. For example, one can have an array of triangular or square plaquettes without any isolated α -site, where the plaquettes can 'touch' each other giving rise to an additional site named δ and having a coordination number four. We refer to Fig. 8 for a display of a disordered arrangement of such building blocks. The analysis proceeds in the same way and the one comes across a varied set of geometries for which the disorder-induced localization (or, a quasiperiodicity driven power law localization) can be suppressed and a full band (or subbands) of extended eigenfunctions can be generated.

VII. CONCLUSION

In conclusion, we have presented a class of topologically disordered array of building blocks described within a tight binding formalism, where delocalization of electronic eigenfunctions occur over either two subbands or

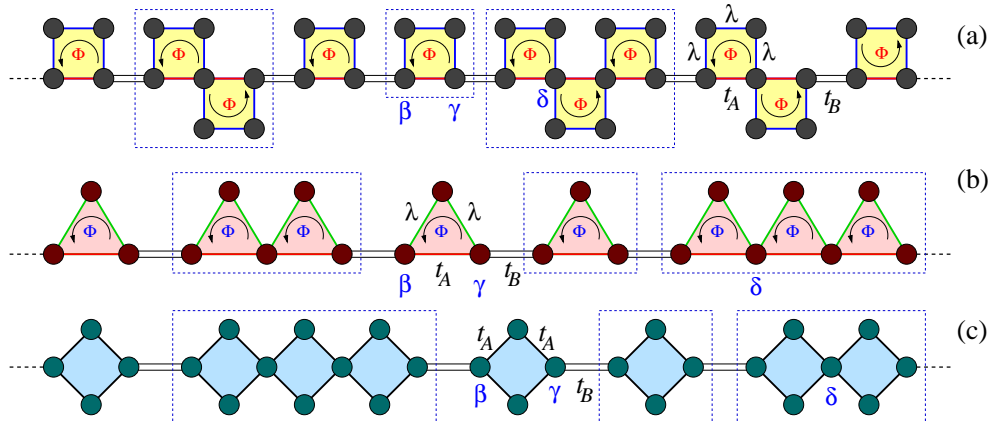


FIG. 8: (Color online) A typical random arrangement of the triangular and square plaquettes where two building blocks can even ‘touch’ each other. There are now three kinds of sites along the backbone, viz., β , γ and δ , the last one having a coordination number four.

over the entire range of allowed energies whenever the lattice parameters are inter-related through certain algebraic relation. We can have absolutely continuous spectrum even for such disordered or quasiperiodic arrangement of the unit cells in such cases. Even an external magnetic field can be used to delocalize the electronic states over a continuous band of energy eigenvalues in certain cases. This aspect leads to the possibility of a flux driven state transition in such low dimensional systems.

Acknowledgments

Biplab Pal gratefully acknowledges a DST-INSPIRE Fellowship, and AC is thankful to DST, India for partial financial support through a PURSE programme of the University of Kalyani.

-
- [1] P. W. Anderson, Phys. Rev. **109**, 1492 (1958).
[2] B. Kramer and A. MacKinnon, Rep. Prog. Phys. **56**, 1469 (1993).
[3] E. Abrahams, P. W. Anderson, D. C. Licciardello, and T. V. Ramakrishnan, Phys. Rev. Lett. **42**, 673 (1979).
[4] D. Vollhardt and P. Wölfle, in Electronic Phase Transitions (eds. W. Hanke and Yu. V. Kopayev) **178** (Elsevier, Amsterdam, 1992).
[5] T. Sperling, W. Bührer, C. M. Aegerter, and G. Maret, Nature Photonics **7**, 48 (2013).
[6] W. Chen and A. A. Clerk, Phys. Rev. A **89**, 033854 (2014).
[7] H. Hu, A. Strybulevych, J. H. Page, S. E. Skipetrov, and B. A. van Tiggelen, Nat. Physics **4**, 945 (2008).
[8] A. Tao, P. Sinsermsuksakul, and P. Yang, Nat. Nanotechnol. **2**, 435 (2007).
[9] A. Christ, Y. Ekinici, H. H. Solak, N. A. Gippus, S. G. Tikhodeev, and O. J. F. Martin, Phys. Rev. B **76**, 201405 (2007).
[10] I. O. Barinov, A. P. Alodzhants, and S. M. Arakelyan, Quantum Electron. **39**, 685 (2009).
[11] M. Grochol and C. Piermarocchi, Phys. Rev. B **78**, 035323 (2008).
[12] B. Damski, J. Zakrzewski, L. Santos, P. Zoller, and M. Lewenstein, Phys. Rev. Lett. **91**, 080403 (2003).
[13] J. Billy, V. Josse, Z. Zuo, A. Bernard, B. Hambrecht, P. Lugan, D. Clément, L. Sanchez-Palencia, P. Bouyer, and A. Aspect, Nature (London) **453**, 891 (2008).
[14] G. Roati, C. D’Errico, L. Fallani, M. Fattori, C. Fort, M. Zaccanti, G. Modugno, M. Modugno, and M. Inguscio, Nature (London) **453**, 895 (2008).
[15] J. Chabé, G. Lemarié, B. Grémaud, D. Delande, P. Szriftgiser, and J. C. Garreau, Phys. Rev. Lett. **101**, 255702 (2008).
[16] S. S. Kondov, W. R. McGehee, J. J. Zirbel, and B. DeMarco, Science **334**, 66 (2011).
[17] R. A. Römer and H. Schulz-Baldes, Europhys. Lett. **68**, 247 (2004).
[18] A. Eilmes, R. A. Römer, and M. Schreiber, Physica B **296**, 46 (2001).
[19] A. Rodríguez, J. Phys. A: Math. Gen. **39**, 14303 (2006).
[20] A. Rodríguez, L. J. Vasquez, and R. A. Römer, Phys. Rev. B **78**, 195107 (2008).
[21] A. Rodríguez, L. J. Vasquez, K. Slevin, and R. A. Römer, Phys. Rev. B **84**, 134209 (2011).
[22] S. D. Pinski, W. Schirmacher, and R. A. Römer, Europhys. Lett. **97**, 16007 (2012).
[23] Lev I. Deych, A. A. Lisyanski, and B. L. Alshuler, Phys. Rev. Lett. **84**, 2678 (2000).
[24] J. W. Kantelhardt and A. Bunde, Phys. Rev. B **66**, 035118 (2002).
[25] M. Titov and H. Schomerus, Phys. Rev. Lett. **95**, 126603 (2005).
[26] P. Mohanty and R. A. Webb, Phys. Rev. Lett. **88**, 146601

- (2002).
- [27] D. H. Dunlap, H-L. Wu, and P. W. Phillips, Phys. Rev. Lett. **65**, 88 (1990).
- [28] T. Sedrakyan, Phys. Rev. B **69**, 085109 (2004).
- [29] T. Sedrakyan and A. Ossipov, Phys. Rev. B **70**, 214206 (2004).
- [30] T. A. Sedrakyan, J. P. Kestner, and S. Das Sarma, Phys. Rev. A **84**, 053621 (2011).
- [31] T. Hakobyan, D. Sedrakyan, A. Sedrakyan, I. Gómez, and F. Domínguez-Adame, Phys. Rev. B **61**, 11432 (2000).
- [32] D. G. Sedrakyan and A. G. Sedrakyan, Phys. Rev. B **60**, 10114 (1999).
- [33] F. Domínguez-Adame, I. Gómez, A. Avakyan, D. Sedrakyan, and A. Sedrakyan, Phys. Status Solidi B **221**, 633 (2000).
- [34] F. A. B. F. de Moura and M. Lyra, Phys. Rev. Lett. **81**, 3735 (1998).
- [35] S. Sil, S. K. Maiti, and A. Chakrabarti, Phys. Rev. B **78**, 113103 (2008).
- [36] A. Rodríguez, A. Chakrabarti, and R. A. Römer, Phys. Rev. B **86**, 085119 (2012).
- [37] V. Kumar and G. Ananthakrishna, Phys. Rev. Lett. **59**, 1476 (1987).
- [38] X. C. Xie and S. Das Sarma, Phys. Rev. Lett. **60**, 1585 (1988).
- [39] B. Pal, S. K. Maiti, and A. Chakrabarti, Europhys. Lett. **102**, 17004 (2013).
- [40] E. Maciá, *Aperiodic Structures in Condensed Matter: Fundamentals and Applications*, and references therein (Series in Condensed Matter Physics, CRC Press, Boca Raton, FL, 2009).
- [41] B. Hopkins, A. N. Poddubny, A. E. Miroshnichenko, and Y. S. Kivshar, Phys. Rev. A **88**, 053819 (2013).
- [42] A. E. Miroshnichenko, S. Flach, and Y. S. Kivshar, Rev. Mod. Phys. **82**, 2257 (2010).
- [43] A. E. Miroshnichenko and Y. S. Kivshar, Phys. Rev. E **72**, 056611 (2005).
- [44] C. Forestiere, G. Miano, C. Serpico, M. d'Aquino, and L. Dal Negro, Phys. Rev. B **79**, 214419 (2009).
- [45] C. Forestiere, G. Miano, G. Rubinacci, and L. Dal Negro, Phys. Rev. B **79**, 085404 (2009).
- [46] D. M. Eigler and E. K. Schweizer, Nature **344**, 524 (1990).
- [47] H. J. Mamin, S. Chang, H. Birk, P. H. Guethner, and D. Ruger, J. Vac. Sci. Technol. B **9**, 1398 (1991).
- [48] C. T. Salling and M. G. Lagally, Science **265**, 502 (1994).
- [49] J. O. Vasseur, P. A. Deymier, G. Frantziskonis, G. Hong, B. Djafari-Rouhani, and L. Dobrzynski, J. Phys.: Condens. Matter **10**, 6051 (1998).
- [50] J. O. Vasseur, P. A. Deymier, L. Dobrzynski, and J. Choi, J. Phys.: Condens. Matter **10**, 8973 (1998).
- [51] B. Pal and A. Chakrabarti, Physica E **60**, 188 (2014).
- [52] A. Chakrabarti and S. Chattopadhyay, e-print arXiv:1112.0871.
- [53] A. D. Stone, J. D. Joannopoulos, and D. J. Chadi, Phys. Rev. B **24**, 5583 (1981).
- [54] R. Farchioni, G. Grosso, and G.P. Parravicini, Phys. Rev. B **85**, 165115 (2012).